Modulation of RNA condensation by the eIF4A RNA helicase

Devin Tauber[1,4], Gabriel Tauber[1,4], Anthony Khong[1,2], Briana Van Treeck[1], Jerry Pelletier[3], and Roy Parker[1,2]*

1. Department of Biochemistry, University of Colorado Boulder, Boulder, CO 80309, USA
2. Howard Hughes Medical Institute, University of Colorado Boulder, Boulder, CO 80309, USA
3. Department of Biochemistry, McGill University, Montreal, QC H3G 1Y6, Canada; The Rosalind and Morris Goodman Cancer Research Center and the Department of Oncology, McGill University, Montreal, QC, Canada
4. These authors contributed equally

*Correspondence: roy.parker@colorado.edu

eTOC Blurb: The RNA helicase eIF4A limits stress granule formation by reducing RNA condensation.

Highlights:

- RNA condensates promote intermolecular RNA-RNA interactions at their surfaces
- eIF4A helicase activity limits the recruitment of RNAs to stress granules in cells
- eIF4A helicase activity reduces the nucleation of stress granules in cells
- Recombinant eIF4A1 inhibits the condensation of RNA *in vitro* in an ATP-dependent manner

Keywords: DEAD-box protein, RNA-RNA interactions, stress granule, ribonucleoprotein

SUMMARY:

Stress granules are condensates of non-translating mRNAs and proteins involved in the stress response and neurodegenerative diseases. Stress granules are proposed to form in part through intermolecular RNA-RNA interactions, although the process of RNA condensation is not well understood. *In vitro*, we demonstrate that the minimization of surface free energy promotes the recruitment and interaction of RNAs on RNA or RNP condensate surfaces. We demonstrate that the ATPase activity of the DEAD-box RNA helicase eIF4A reduces RNA recruitment to RNA condensates *in vitro* and in cells, as well as limiting stress granule formation. This defines a new function for eIF4A, and potentially other RNA helicases, to limit thermodynamically favored intermolecular RNA-RNA interactions in cells, thereby allowing for proper RNP function.

INTRODUCTION

Eukaryotic cells contain ribonucleoprotein (RNP) granules in the nucleus and cytosol, including P-bodies (PBs) and stress granules (SGs) (Anderson and Kedersha, 2006; Banani et al., 2017). Stress granules are cytosolic RNP condensates composed of non-translating mRNPs, which are involved in the stress response, neurodegeneration and viral infection (Protter and Parker, 2016; Advani and Ivanov, 2019). SGs typically form in response to translational shutoff induced by noxious stimuli such as arsenite, heat shock, and endogenous inflammatory molecules like prostaglandins, which all lead to phosphorylation of eIF2α and the activation of the integrated stress response (Aulas et al., 2017; Tauber and Parker, 2019). Stress granules can also form independently of eIF2α phosphorylation in response to inhibition of the eIF4F complex or high salt stress (Aulas et al., 2017). SGs and other RNP condensates are thought to form in part through multimeric RNA binding proteins crosslinking RNPs into larger networks (Banani et al., 2017; Shin and Brangwynne, 2018).

Recent evidence has emerged showing that intermolecular RNA-RNA interactions are involved in SG formation. SGs require a substantial pool of non-translating RNA to form (Protter and Parker, 2016). Thus, elevating the non-translating RNA concentration by injecting exogenous RNA induces SGs (Bounedjah et al., 2014). Furthermore, certain RNAs can seed foci in human cell lysates that recruit many SG proteins (Fay et al., 2017). Strikingly, modest concentrations of yeast total RNA readily condense in physiological salt and polyamine conditions, recapitulating the SG transcriptome in a protein-free context (Khong et al., 2017; Van Treeck et al., 2018), arguing that RNA-RNA interactions contribute to SG formation.

Roles for RNA in forming, maintaining, and organizing RNP condensates are not limited to SGs. For example, nuclear paraspeckles require the lncRNA *NEAT1* to form (Fox and Lamond, 2010; West et al., 2016). Moreover, specific RNA-RNA interactions between *NEAT1* domains may be important for paraspeckle formation and integrity (Lu et al., 2016; Lin et al., 2018). Similarly, the formation of RNA foci of repeat expansion RNAs has been suggested to occur through an RNA based condensation (Jain and Vale, 2017). In the *Drosophila* embryo, homotypic intermolecular base-pairing between *oskar* or *bicoid* mRNAs determines whether the RNAs will localize to RNP granules in the anterior or the posterior of the embryo, promoting polarity establishment (Ferrandon et al., 1997; Jambor et al., 2011). Specific intermolecular interactions between mRNAs may also be important for their recruitment to polarized RNP granules in *Ashbya gossypii* (Langdon et al., 2018). Despite their relevance to RNP condensate formation in cells, the properties of condensed RNA are not well-understood.

The diversity of intermolecular RNA-RNA interactions relevant to RNP granules and the low barriers for RNA condensation *in vitro* (Van Treeck and Parker, 2018) are consistent with RNA-based assemblies playing myriad cellular roles, but also create a need for the cell to regulate the processes of RNA condensation and recruitment. One possible modulatory mechanism would be the activity of RNA chaperones like RNA helicases, a class of ATPases that unwind RNA-RNA interactions (Jarmoskaite and Russell, 2014) and could thereby limit RNA condensation in the cell. Notably, virtually all RNP granules contain RNA helicases (Charroux et al., 1999; Saitoh et al., 2004; Dias et al., 2010; Hubstenberger et al., 2013; Calo et al., 2015; Tu and Barrientos, 2015; Jain et al., 2016; Hubstenberger et al., 2017), and these helicases are often conserved across eukaryotes (Linder and Fuller-Pace, 2013; Jarmoskaite and Russell, 2014). For

example, SGs contain multiple conserved helicases, including eIF4A/Tif1 and DDX3/Ded1, in both mammals and yeast, respectively (Jain et al., 2016). Similarly, RNA helicases are found localized in bacterial RNP granules as well (Taghbalout and Rothfield, 2008; Al-Husini et al., 2018).

Here, we examine RNA condensation and its modulation by the essential translation initiation factor, SG protein, and DEAD-box RNA helicase eIF4A *in vitro* and in the cell. We show that RNA and RNP condensates stably interact with other RNAs or RNA-based condensates at their surfaces promoting RNA condensate assembly. In contrast, we demonstrate that eIF4A limits the recruitment of RNAs to SGs through its helicase function, combating this process. Moreover, we show that eIF4A helicase activity, separate from translational effects, can prevent the formation of SGs in cells, limits the interfacial interactions of PBs and SGs, and reduces the condensation of RNA in physiological conditions *in vitro*. Together, these data argue eIF4A functions as an "RNA decondensase," to limit inappropriate, but thermodynamically favored intermolecular RNA-RNA interactions. Such an "RNA decondenase" function is analogous to the role of protein chaperones in limiting inappropriate intermolecular protein-protein interactions.

RESULTS

To examine how the nature of RNA interactions affects RNA condensation and the material properties of RNA condensates, we first examined the co-assembly of pairwise combinations of the homopolymer RNAs polyU, polyC, or polyA, which individually condense into RNA droplets of increasing viscosity, respectively (Aumiller et al., 2016; Van Treeck et al., 2018). The differential recruitment of short fluorescent oligonucleotides into homopolymer assemblies (Figure S1A & B) allowed us to distinguish between homopolymer condensates. Notably, the robustness of recruitment tended to coincide with the relative strengths of intermolecular RNA-RNA interactions between the oligonucleotides and the homopolymer scaffolds, with the most efficient recruitment occurring when the oligonucleotide could form Watson-Crick base pairs with the condensate scaffold. Some non-complementary RNAs were robustly recruited to condensate surfaces instead, such as oligoG with polyA or PTR with polyC (Figure S1A & B).

Examination of the condensation of mixed homopolymers revealed that increasing the net RNA-RNA interaction strength through extensive base-pairing between polyA and polyU leads to gelatinous aggregates containing both homopolymers (Figure 1A). In contrast, mixtures of polyC and polyU spontaneously self-organize into patterned networks of alternating, immiscible polyC and polyU droplets (Figure 1A). A similar, but less organized, flocculation of polyA and polyC assemblies occurred (Figure 1A). These observations demonstrate that RNA-RNA interaction strengths determine the material phase of RNA condensates and that differential interaction strengths can lead to the homotypic clustering and specific compartmentalization of

RNAs. Such sequence-specific organization of RNAs in condensates may be relevant to the homotypic clustering and/or organization of RNAs in RNP condensates in cells, such as the *Drosophila* germ granule (Trcek et al., 2015).

Three observations indicate that RNA condensates associate with one another at interfaces to reduce the free energy of the system. First, the polyC/polyU interface is elongated, deforming the droplets (Figure 1A), indicating that the polyC/polyU interface is lower-energy than either homopolymer/solvent phase boundary. A similar, but less extensive, docking of polyA and polyC condensates is also observed (Figure 1A), also consistent with interfacial interactions reducing surface free energy. Second, time-lapse microscopy shows that polyC and polyU condensates are associated from an early time point and appear to nucleate off of each other (Movie S1), indicating that their association is not merely due to the crowding of droplets. Third, polyC and polyU droplets remain associated with each other following mechanical disruption (Figure S1C), indicative of a bona fide physical interaction between the two condensate types.

The minimization of surface energy by heterotypic RNA condensate interactions raised the possibility that the recruitment of RNAs to RNA/RNP condensate surfaces would also be thermodynamically favored. To test this possibility, we condensed polyA, polyC, or polyU in the presence of fluorescently labeled mRNAs. We observed that most mRNAs localized to the surfaces of all three homopolymer condensates, though some RNAs were internalized in polyC (Figures 1B and S1D). Similarly, we observed that SGs isolated from mammalian cells (Figures 1C & D), and RNA assemblies formed from a myotonic dystrophy associated CUG repeat RNA

(known to form RNA condensates in cells; Jain and Vale, 2017), recruit RNA to their surfaces *in vitro* (Figure 1E). Thus, a diversity of RNA and RNP assemblies recruit RNAs to their surfaces.

We also observed that the condensation of *pgc* RNA with both polyC and polyU led to the formation of polyC/polyU multi-phase assemblies (Figure 1F) with *pgc* RNA localized robustly to the polyC/polyU interface. This observation argues that specific RNAs might act similarly to surfactants or interfacial shells between distinct RNA/RNP condensate phases, and thereby stabilize multi-phase RNP condensates like the nucleolus (Feric et al., 2016).

Three observations demonstrate that the recruitment of RNAs to the surface of an RNA condensate leads to enhanced interaction between those RNAs and the formation of an RNA shell of enhanced stability enveloping the underlying RNA condensate. First, the surface ring of *pgc* mRNAs recruited to polyA condensates is more stable following dilution than the underlying polyA assembly, persisting for several minutes longer (Figures 2A & B, Movie S2). Second, while the internal polyA droplet (visualized by fluorescent oligoU) is somewhat dynamic by FRAP analysis (mobile fraction, m.f. = 0.29 ± 0.02), the *pgc* shell shows virtually no recovery (m.f. = 0.02 ± 0.02), implying that the shell is immobile (Figure S2). Third, using 4'-aminomethyltrioxsalen, which crosslinks RNA duplexes in UV light (Frederikson and Hearst, 1979), we observed that *pgc-pgc* crosslinking, analyzed on denaturing gels, increased when assembled on the surface of polyA condensates as compared to in dilute solution, or even when compared to homotypic, self-assembled *pgc* gels (Figures 2C-E).

These observations demonstrate that the surfaces of RNA assemblies are favored sites of RNA interaction due to the minimization of surface free energy. Thus, the favorable binding of RNAs onto the surface of an RNP granule can concentrate RNAs/RNPs, thereby promoting additional intermolecular RNA/RNP interactions, further stabilizing the system (Figure 2F). This suggests that intermolecular RNA interactions will be thermodynamically favored in cells, and therefore mechanisms must exist to limit the recruitment of RNAs onto the surfaces of RNP granules. We hypothesized that one or more RNA helicases would act as "RNA decondensases" in cells by dissociating the intermolecular RNA-RNA interactions that promote RNP condensation.

eIF4A helicase activity limits RNP partitioning into stress granules

To examine the role of helicases in limiting RNA condensation, we focused on SGs. Multiple helicases partition into SGs (Chalupníková et al., 2008; Hillicker et al., 2011; Jain et al., 2016; Markmiller et al., 2018) with eIF4A1, an essential, highly-conserved component of the eIF4F translation initiation complex, being the most abundant in both U-2 OS and HeLa cell lines (Figure 3A; Beck et al., 2011; Itzhak et al., 2016). eIF4A may have additional functions since eIF4A1 is present at ~10X the concentration of other eIF4F components (Itzhak et al., 2016), with between 5-50 molecules of eIF4A1 for each mRNA in U-2 OS and HeLa cells (calculations in *Methods*).

eIF4A1 partitions into SGs during $NaAsO_2$ stress, and on average extends further into the cytosol then the traditional SG marker, G3BP1 (Figure 3B), indicating eIF4A1 is enriched at the

periphery of SGs. In contrast, DDX1, another SG RNA helicase, is uniformly distributed within the granule and overlaps with G3BP1 (Figure 3B). The peripheral concentration of eIF4A1 in SGs is consistent with eIF4A1 modulating the interactions of RNAs with the surfaces of SG.

If eIF4A limits the condensation of RNAs into stress granules, then eIF4A inhibition should increase RNA partitioning into SGs. To separate the effects of eIF4A inhibition on translation initiation from its helicase function, we first treated U-2 OS cells with arsenite to inhibit bulk translation initiation through eIF2α phosphorylation, then added hippuristanol for 30', which inhibits the helicase activity of eIF4A (Lindqvist et al., 2008). We then examined the partitioning of mRNAs into SGs by single molecule FISH (smFISH).

We observed that the fraction of *TFRC*, but not *POLR2A*, mRNAs associated with SGs increased after hippuristanol treatment (Figure 3C). Since there are additional helicases in SGs, we also examined mRNA partitioning into arsenite-induced SGs following ATP depletion, which would inhibit all ATP-dependent RNA helicases. After ATP depletion, we observed both *TFRC* and *POLR2A* mRNAs increased their partitioning into SGs, consistent with additional RNA helicases, or other ATP-dependent mechanisms, limiting mRNA condensation into SGs.

To examine the role of eIF4A helicase activity on RNA partitioning into SG independently of its role in translation in a second context, we also measured the partitioning of the SG-enriched (Khong et al., 2017) *NORAD* lncRNA, which is never translated, in the presence of arsenite, hippuristanol, or Pateamine A (PatA), which inhibits eIF4A's function in translation initiation without affecting its helicase activity (Bordeleau et al., 2005; Bordeleau et al., 2006).

We observed that the *NORAD* RNA increased in SGs during hippuristanol treatment, as compared to arsenite or PatA (Figure 3D). Similarly, we observed bulk mRNA and the abundant RNA binding protein G3BP1 partitioned more robustly to SGs in hippuristanol-treated cells as assessed by oligo(dT) FISH or IF, respectively (Figure S3).

These observations demonstrate that the RNA helicase activity of eIF4A1, independent of its role in translation, limits the accumulation of RNPs in SGs. We suggest that RNAs not affected by eIF4A might be limited from entering stress granules by other RNA helicases, or might be primarily targeted to SGs by proteins.

eIF4A helicase activity limits stress granule formation

We hypothesized that limiting intermolecular RNA interactions through eIF4A and other helicases would affect not only the recruitment of mRNPs to SGs, but also intermolecular RNA-RNA interactions between mRNPs that contribute to SG assembly. To test this possibility, we took advantage of the observation that during arsenite stress, SGs do not form in cells lacking the abundant RNA binding proteins G3BP1/G3BP2, which provide protein-protein interactions to assist SG assembly through G3BP dimerization (Tourrière et al., 2003; Kedersha et al., 2016). We hypothesized that inhibition of eIF4A helicase activity would compensate for the absence of G3BP in SG formation by promoting increased levels of intermolecular RNA-RNA interactions. Thus, we examined SG formation in WT and ΔΔG3BP1/2 cell lines during arsenite stress, where we altered eIF4A function after 30' of arsenite stress with either hippuristanol, blocking eIF4A helicase activity, or PatA as a negative control. Puromycin labeling revealed that translation was

repressed similarly in all three conditions, indicating that any effects are not due to additional translational repression (Figure S4A).

Importantly, hippuristanol treatment partially restored SG formation in the ΔΔG3BP1/2 cell lines as assessed by PABPC1 IF, but PatA treatment did not (Figure 4A). These PABPC1 foci are SGs since they are sensitive to cycloheximide (Figure S5), which blocks SG formation by trapping mRNAs in polysomes (Kedersha et al., 2000), they do not colocalize with PBs, and they contain multiple SG proteins and the SG-enriched mRNA *AHNAK* (Figure S5, S4G). Depletion of eIF4A1, the predominant form of eIF4A in U-2 OS cells (Figure 3A), by siRNAs (Figure S4B) also led to the restoration of SGs in the ΔΔG3BP1/2 cell line during arsenite treatment (Figure 4B). This demonstrates that the helicase function of eIF4A limits SG formation.

In principle, eIF4A could limit SG formation by limiting intermolecular RNA-RNA interactions, or by increasing the off-rate of RNA-binding proteins contributing to SG assembly. However, inhibition of eIF4A helicase activity with hippuristanol does not alter the exchange rates of G3BP1 (Figure S4F), consistent with eIF4A altering SG formation by promoting the dissociation of intermolecular RNA-RNA interactions.

Since SGs were only partially restored with hippuristanol, we also depleted cells of ATP after 30' of arsenite stress, when ATP is no longer necessary to release mRNAs from polysomes (Jain et al., 2016), to inhibit all ATP-dependent RNA helicases. Depletion of ATP restored SG formation more robustly than hippuristanol in ΔΔG3BP1/2 cells (Figure 4A). We interpret these observations to signify that in addition to the helicase activity of eIF4A, other ATP-dependent

mechanisms, including RNA helicases, limit SG formation. Moreover, the observation that ATP depletion following translational arrest promotes SG formation is consistent with RNP condensation into SGs being an energetically favored process.

Since inhibiting the helicase activity of eIF4A increased SG formation independent of its role in translation, we predicted that over-expression of eIF4A would limit intermolecular RNA-RNA interactions and thereby limit SG formation. To test this, we over-expressed Myc tagged eIF4A1 in wildtype U-2 OS cells (Figure S4C) by transient transfection. We then examined whether cells with over-expressed eIF4A1 could still form SGs in response to arsenite treatment. We observed that cells with over-expression of eIF4A1 failed to form SGs, although those cells still robustly repressed translation (Figure 4C, 4D, S4D, S4E), consistent with eIF4A limiting RNA condensation into SGs.

Because other RNA helicases likely function as RNA decondensases, we decided to test if a closely related DEAD-box helicase, DDX19A/DBP5 (Cencic and Pelletier, 2016), could prevent SG formation in an analogous manner to eIF4A1. DDX19A over-expression has been reported to inhibit the formation of SGs induced by the transcriptional inhibitor tubercidin by an unknown mechanism (Hochberg-Laufer et al., 2019). We reasoned that DDX19A could be acting as an RNA decondensase since its helicase core sequence is highly similar to eIF4A. Strikingly, mCherry-DDX19A overexpression inhibited arsenite induced SG formation to a similar extent as eIF4A, while over-expression of mCherry alone had no effect on SG formation (Figure 4D). This effect is independent of translation repression since cells with over-expressed DDX19A still repressed translation equally in response to arsenite treatment (Figure S4E). This

demonstrates that multiple different helicases can limit RNA condensation and SG formation, which is consistent with ATP depletion having a larger effect on SG formation than inhibition of eIF4A alone (Figure 4).

eIF4A helicase activity limits docking of P bodies with stress granules

Heterotypic RNP granules, like SGs and PBs (Kedersha et al., 2005) or nuclear speckles and paraspeckles (Fox et al., 2002), are observed to dock in cells. Since heterotypic RNA condensates minimize their surface free energy through RNA-RNA docking interactions (Figure 1A), we hypothesized that PB/SG interfaces might occur through intermolecular RNA interactions. If so, the docking of PBs and SGs would be predicted to be modulated by eIF4A. To test this, we quantified PB/SG interfaces in cells treated with arsenite, either alone, or with hippuristanol or PatA treatment. We observed that PB/SG interfaces increased with hippuristanol, but not PatA treatment (Figure 5). This observation argues that eIF4A helicase activity also limits docking interactions between the heterotypic PBs and SGs.

eIF4A1 is sufficient to limit RNA condensation *in vitro*

To determine if eIF4A was sufficient to limit RNA condensate formation *in vitro*, we examined how recombinant eIF4A1 affected the formation of RNA condensates *in vitro*. We assessed RNA condensate formation by observing RNA condensates with differential interference contrast (DIC) microscopy and also by the recruitment of a fluorescent RNA, PTR, to RNA condensates formed from total yeast RNA in physiological K^+ and polyamine

concentrations. We performed these experiments with eIF4A at 10 μM, which is its approximate concentration in the cytosol (Itzhak et al., 2016) and with RNA at 150 μg/ml, which we have estimated is the concentration of exposed ORF RNA during a stress response (Van Treeck et al., 2018). We then examined the formation of RNA condensates over time in the presence or absence of recombinant eIF4A1, with or without ATP or the non-hydrolyzable ATP analog adenylyl-imidodiphosphate (ADPNP).

An important result was that RNA condensation, as assessed by either DIC microscopy (Figure S6) or by the recruitment of the fluorescent RNA (Figure 6), was strongly reduced by the addition of eIF4A1 and ATP. In contrast, the addition of ATP alone, ADPNP, or eIF4A plus ADPNP, had smaller effects on RNA condensation (Figure 6). eIF4A in the presence of ADPNP might partially inhibit RNA condensation as a monomeric RNA binding protein since, when bound to ADPNP, eIF4A retains its ability to bind RNA (Lorsch and Herschlag, 1998). However, since eIF4A1 binds RNA to a similar degree in the presence of either ATP or ADPNP (Lorsch and Herschlag, 1998), these observations argue that ATP hydrolysis, and thus the helicase activity, of eIF4A1 most strongly inhibits RNA condensation. Therefore, the eIF4A1 helicase is sufficient to decondense RNA by limiting intermolecular RNA-RNA interactions.

DISCUSSION

Several observations argue that RNA condensation into RNP granules is a thermodynamically favored process that is countered by energy-consuming processes in the cell. First, multiple distinct RNAs are robust at self-assembly *in vitro*, including under physiological conditions of salts and polyamines (Figure 1; Figure S1; Aumiller et al., 2016; Jain and Vale, 2017; Langdon et al., 2018; Van Treeck et al., 2018). Moreover, RNA generally requires lower concentrations to condense *in vitro* than intrinsically disordered proteins (Van Treeck and Parker, 2018). Second, we observe that condensates of different RNA composition can interact to reduce the surface free energy of the RNA condensates (Figure 1). Third, RNA condensates or stress granules from cells recruit RNAs to their surface *in vitro* (Figure 2). Moreover, in cells, depletion of ATP promotes the condensation of untranslated mRNPs into SGs (Figure 3C), even in the absence of protein factors normally are required for SG formation (Figure 4A), demonstrating cells utilize energy to limit SG formation.

In vitro we observe that the recruitment of RNAs to the surface of an RNA condensate creates a high local concentration, which promotes the formation of additional interactions between the molecules to further stabilize the RNA assembly (Figure 2). This creates a positive feedback loop in RNA condensation. Thus, RNA condensation has the potential to create an "RNA entanglement catastrophe" wherein extensive RNA condensation would limit the proper distribution and function of RNAs. An implication of these observations is that cells must contain mechanisms to limit the condensation of RNA.

We present several lines of evidence arguing that eIF4A functions to limit cytosolic RNA condensation through its role as a general RNA helicase. First, arsenite coupled with eIF4A1 knockdown or treatment of cells with hippuristanol, but not PatA, restores SG formation in cells lacking G3BP without changes in translational repression (Figure 4A & B). Second, overexpression of eIF4A1 limits SG formation, although translation remains repressed (Figure 4C, S4D). Third, inhibition of the helicase activity of eIF4A during arsenite stress enriches some RNAs in stress granules (Figures 3 and S3). Fourth, inhibition of eIF4A helicase activity with hippuristanol increases PB/SG docking events (Figure 5). Finally, recombinant eIF4A1 is able to limit RNA condensation *in vitro* in an ATP-dependent manner (Figure 6). Since inhibition of eIF4A helicase activity with hippuristanol does not alter the exchange rates of G3BP1 (Figure S4), we interpret these observations to suggest that eIF4A limits RNA condensation by the disassembly of intermolecular RNA-RNA interactions.

A general role for eIF4A in limiting RNA condensation in the cytosol provides an explanation for why eIF4A1 is such an abundant protein and present at ~10X higher concentrations than other translation initiation factors (Itzhak et al., 2016). Since ATP depletion is more effective at rescuing SG formation in cell lines lacking G3BP (Figure 4A), and has a larger effect on mRNA recruitment to SGs during arsenite stress (Figure 3C), we suggest that additional ATP-dependent RNA decondenases, including other helicases found associated with SGs (Figure 3A), also limit RNP condensation into SGs. Consistent with other helicases limiting SG formation, we demonstrate over-expression of DDX19A, which is closely related to eIF4A, can limit SG formation without restoring translation (Figure 4). Interestingly, knockout of the DHX36 helicase has been shown to lead to increased SG formation (Sauer et al., 2019), but this

appears to be due to constitutive activation of PKR and increased translation repression. An important area of future work will be identifying additional helicases that limit RNA condensation and determining if they act in RNA specific manners.

The generality and thermostability of RNA condensation predict it will be relevant to other RNP granules. Indeed, observations in the literature are consistent with other RNA helicases functioning to limit RNAs being retained in RNA condensates. For example, knockdown of the RNA helicase UAP56/DDX39B (which is also related to eIF4A; Cencic and Pelletier, 2016), leads to increased accumulation of polyA$^+$ RNA or fully spliced beta-globin mRNA in nuclear speckles (Dias et al., 2010), which are RNP condensates formed near sites of transcription (Galganski et al., 2017). Similarly, knockdown of the Upf1 RNA helicase leads to retention of nascent transcripts in nuclear foci with DNA (Singh et al., 2019), where a high local concentration of nascent RNA might lead to RNA entanglements. These results suggest that helicases may be generally required to prevent the trapping of RNAs in thermodynamic energy wells at RNP granules. Additional mechanisms cells could utilize to limit RNA condensation include ribosome association, abundant RNA binding proteins, and RNA modifications that limit the stability of RNA-RNA interactions.

A role for eIF4A, and other general RNA helicases, in limiting RNA condensation can be considered analogous to protein chaperones, such as Hsp70, limiting the aggregation of misfolded proteins. Multiple protein chaperones, including Hsp70 proteins, bind to unfolded proteins and use the energy of ATP hydrolysis to disassemble aberrant interactions, thereby allowing for refolding of the protein and the solubilization of protein aggregates (Mogk et al.,

2018). We suggest that RNA condensation and inappropriate aggregation occurs when the amount of exposed RNA in the cell exceeds the capacity of the cellular machinery limiting RNA condensation. Under these cellular conditions, general RNA helicases would bind to condensed or aggregated RNAs, unwind intermolecular RNA-RNA interactions promoting RNA decondensation. Thus, the intrinsic aggregation properties of both proteins and RNAs are countered by abundant cellular machines that keep these macromolecules correctly folded and dispersed for proper function.

Acknowledgements: We thank the Parker lab, Amy Buck, and Olke Uhlenbeck for discussions. We thank the University of Colorado BioFrontiers Institute Cell Culture Facility and the BioFrontiers Institute Advanced Light Microscopy Core Facility (NIST-CU cooperative agreement 70NANB15H226 and NIH 1S10RR026680-01A1), John Rinn and Matt Disney for providing reagents. mCherry-DDX19A plasmids were a kind gift from Yaron Shav-Tal. This work was funded by NSF SCR training grant T32GM08759 (to D.T.), a Banting Postdoctoral Fellowship (to A.K.), NIH GM045443 (to R.P.) and the Howard Hughes Medical Institute.

Author contributions: D.T., G.T., and R.P. conceived the project. D.T., G.T., and A.K. designed, performed, and analyzed experiments. J.P. provided intellectual input and materials. D.T., G.T., and R.P. wrote the manuscript.

Competing interests: The authors declare no competing interests.

Data and materials availability: All data is available in the manuscript or supplementary materials.

References

Advani, V.M., and Ivanov, P. (2019). Translational Control under Stress: Reshaping the Translatorme. Bioessays *41*, e1900009. doi: 10.1002/bies.201900009.

Al-Husini, N., Tomares, D.T., Bitar, O., Childers, W.S., Schrader, J.M. (2018). α-Proteobacterial RNA Degradosomes Assemble Liquid-Liquid Phase-Separated RNP Bodies. Mol. Cell 71, 1027–1039.

Anderson, P., and Kedersha, N. (2006). RNA granules. J. Cell Biol. *172*, 803-808.

Aulas, A., Fay, M.M., Lyons, S.M., Achorn, C.A., Kedersha, N., Anderson, P., and Ivanov, P. (2017). Stress-specific differences in assembly and composition of stress granules and related foci. J. Cell Sci. *130*, 927–937.

Aumiller, W.M., Jr., Pir Cakmak, F., Davis, B.W., and Keating, C.D. (2016). RNA-Based Coacervates as a Model for Membraneless Organelles: Formation, Properties, and Interfacial Liposome Assembly. Langmuir *32*, 10042–10053.

Banani, S.F., Lee, H.O., Hyman, A.A., and Rosen, M.K. (2017). Biomolecular condensates: organizers of cellular biochemistry. Nat. Rev. Mol. Cell Biol. *18*, 285-298.

Beck, M., Schmidt, A., Malmstroem, J., Classen, M., Ori, A., Szymborska, A., Herzog, F., Rinner, O., Ellenberg, J., and Aebersold, R. (2011). The quantitative proteome of a human cell line. Mol. Syst. Biol. *7*, 549.

Bordeleau, M.E., Cencic, R., Lindqvist, L., Oberer, M., Northcote, P., Wagner, G., and Pelletier, J. (2006). RNA-mediated sequestration of the RNA helicase eIF4A by pateamine A inhibits translation initiation. Chem. Biol. *13*, 1287-1295.

Bordeleau, M.E., Matthews, J., Wojnar, J.M., Lindqvist, L., Novac, O., Jankowsky, E., Sonenburg, N., Northcote, P., Teesdale-Spittle, P., and Pelletier, J. (2005). Stimulation of mammalian translation initiation factor eIF4A activity by a small molecule inhibitor of eukaryotic translation. Proc. Nat. Acad. Sci. USA *102*, 10460-10465.

Bounedjah, O., Desforges, B., Wu, T.D., Pioche-Durieu, C., Marco, S., Hamon, L., Curmi, P.A., Guerquin-Kern, J.L., Pie´ trement, O., and Pastre´ , D. (2014). Free mRNA in excess upon polysome dissociation is a scaffold for protein multimerization to form stress granules. Nucleic Acids Res. *42*, 8678–8691.

Calo, E., Flynn, R.A., Martin, L., Spitale, R.C., Chang, H.Y., and Wysocka, J. (2015). Nuclear helicase DDX21 coordinates transcription and ribosomal RNA processing. Nature *518*, 249-253.

Cencic, R., and Pelletier, J. (2016). Hippuristanol – a potent steroid inhibitor of eukaryotic initiation factor 4A. Translation (Austin) *4*, e1137381. doi: 10.1080/21690731.2015.1137381

Chalupníková, K., Lattmann, S., Selak, N., Iwamoto, F., Fujiki, Y., and Nagamine, Y. (2008). Recruitment of the RNA helicase RHAU to stress granules via a unique RNA-binding domain. J. Biol. Chem. *283*, 35186-98.

Charroux, B., Pellizzoni, L., Perkinson, R.A., Shevchenko, A., Mann, M., and Dreyfuss, G. (1999). Gemin3: A novel DEAD box protein that interacts with SMN, the spinal muscular atrophy gene product, and is a component of gems. J. Cell Biol. *147*, 1181–1194.

Dias, A.P., Dufu, K., Lei, H., and Reed, R. (2010). A role for TREX components in the release of spliced mRNA from nuclear speckles. Nat. Commun. *1*, 97 https://doi.org/10.1038/ncomms1103.

Fay, M.M., Anderson, P.J., and Ivanov, P. (2017). ALS/FTD-associated C9ORF72 repeat RNA promotes phase transitions in vitro and in cells. Cell Rep. *21*, 3573–3584.

Feric, M., Vaidya, N., Harmon, T.S., Mitrea, D.M., Zhu, L., Richardson, T.M., Kriwacki, R.W., Pappu, R.V., and Brangwynne, C.P. (2016). Coexisting liquid phases underlie nucleolar subcompartments. Cell *165*, 1686-1697.

Ferrandon, D., Koch, I., Westhof, E., and Nüsslein-Volhard, C. (1997). RNA- RNA interaction is required for the formation of specific bicoid mRNA 3' UTR-STAUFEN ribonucleoprotein particles. EMBO J. *16*, 1751–1758.

Fox, A.H., Lam, Y.W., Leung, A.K., Lyon, C.E., Andersen, J., Mann, M., and Lamond, A.I. (2002). Paraspeckles: a novel nuclear domain. Curr. Biol. *8*, 13-25.

Frederikson, S., and Hearst, J.E. (1979). Binding of 4'-aminomethyl 4,5',8-trimethyl psoralen to DNA, RNA, and protein in HeLa cells and *Drosophila* cells. Biochim. Biophys. Acta *563*, 343-355.

Galganski, L., Urbanek, M.O., and Krzyzosiak, W.J. (2017). Nuclear speckles: molecular organization, biological function and role in disease. Nucleic Acids Res. *45*, 10350–10368.

Hillicker, A., Gao, Z., Jankowsky, E., and Parker, R.. The DEAD-box protein Ded1 modulates translation by the formation and resolution of an eIF4F-mRNA complex. Mol. Cell *43*, 962-72.

Hochberg-Laufer, H., Schwed-Gross, A., Neuebauer, K.M., and Shav-Tal, Y. (2019). Uncoupling of nucleo-cytoplasmic RNA export and localization during stress. Nucleic Acids Res. *47*, 4778-4797.

Hubstenberger, A., Noble, S.L., Cameron, C., and Evans, T.C. (2013). Translation repressors, an RNA helicase, and developmental cues control RNP phase transitions during early development. Dev. Cell *27*, 161–173.

Hubstenberger, A., Courel, M., Bénard, M., Sonquere, S., Ernoult-Lange, M., Chouaib, R., Yi, Z., Morlot, J.B., Munier, A., Fradet, M., *et al*. (2017). P-Body Purification Reveals the Condensation of Repressed mRNA Regulons. Mol. Cell *68*, 144-157.

Itzhak, D.N., Tyanova, S., Cox, J., and Borner, G.H.H. (2016). Global, quantitative and dynamic of protein subcellular localization. eLife *5*, e16950.

Jain, A., and Vale, R.D. (2017). RNA phase transitions in repeat expansion disorders. Nature *546*, 243-247.

Jain, S., Wheeler, J.R., Walters, R.W., Agrawal, A., Barsic, A., and Parker, R. (2016). ATPase-modulated stress granules contain a diverse proteome and substructure. Cell *164*, 487-489.

Jambor, H., Brunel, C., and Ephrussi, A. (2011). Dimerization of oskar 3' UTRs promotes hitchhiking for RNA localization in the Drosophila oocyte. RNA *17*, 2049–2057.
Jarmoskaite, I., and Russell, R. (2014). RNA helicase proteins as chaperones and remodelers. Ann. Rev. Biochem. *83*, 697-725.

Kedersha, N., Cho, M.R., Lei, W., Yacono, P.W., Chen, S., Gilks, N., Golan, D.E., and Anderson, P. (2000). Dynamic shuttling of Tia-1 accompanies the recruitment of mRNA to stress granules. J. Cell Biol. *151*, 1257-1268.

Kedersha, N., Panas, M.D., Achorn, C.A., Lyons, S., Tisdale, S., Hickman, T., Thomas, M., Lieberman, J., McInnery, G.M., Ivanov, P., and Anderson, P. (2016). G3BP-Caprin1-USP10 complexes mediate stress granule condensation and associate with 40S subunits. J. Cell Biol. *212*, 845-60.

Kedersha, N., Stoecklin, G., Ayodele, M., Yacono, P., Lykke-Andersen, J., Fritzler, M.J., Scheuner, D., Kaufman, R.J., Golan, D.E., and Anderson, P. (2005). Stress granules and processing bodies are dynamically linked sites of mRNP remodeling. J. Cell Biol. *169*, 871-84.

Khong, A., Jain, S., Matheny, T., Wheeler, J.R., and Parker, R. (2017). Isolation of mammalian stress granule cores for RNA-seq analysis. Methods *137*, 49-54.

Khong, A., Matheny, T., Jain, S., Mitchell, S.F., Wheeler, J.R., and Parker, R. (2017). The Stress Granule Transcriptome Reveals Principles of mRNA Accumulation in Stress Granules. Mol. Cell *68*, 808- 820.

Langdon, E.M., Qiu, Y., Ghanbari Niaki, A., McLaughlin, G.A., Weidmann, C.A., Gerbich, T.M., Smith, J.A., Crutchley, J.M., Termini, C.M., Weeks, K.M., et al. (2018). mRNA structure determines specificity of a polyQ-driven phase separation. Science *360*, 922–927.

Linder, P., and Fuller-Pace, F.V. (2013). Looking back on the birth of DEAD-box RNA helicases. Biochim. Biophys. Acta *1829*, 750-5.

Lindqvist, L., Oberer, M., Reibarkh, M., Cencic, R., Bordeleau, M.E., Vogt, E., Marintchev, A., Tanaka, J., Fagotto, F., Altmann, M., Wagner, G., and Pelletier, J. (2008). Selective pharmacological targeting of a DEAD-box helicase. PLoS One *3*, e1583.

Lorsch, J.R., and Herschlag, D. (1998). The DEAD box protein eIF4A. 1. A minimal kinetic and thermodynamic framework reveals coupled binding of RNA and nucleotide. Biochemistry *37*, 2180-2193.

Markmiller, S., Soltanieh, S., Server, K.L., Mak, R., Jin, W., Fang, M.Y., Luo, E.C., Krach, F., Yang, D., Sen, A., *et al*. (2018). Context-dependent and disease-specific diversity in protein interactions within stress granules. Cell *172*, 590-604.

Mogk, A., Bukau, B., Kampinga, H.H. (2018). Cellular handling of protein aggregates by disaggregation machines. Mol. Cell *69*, 214-226.

Protter, D.S.W., and Parker, R. (2016). Principles and Properties of Stress Granules. Trends Cell Biol. *26*, 668-679.

Saitoh, N., Spahr, C.S., Patterson, S.D., Bubulya, P., Neuwald, A.F., and Spector, D.L. (2004). Proteomic analysis of interchromatin granule clusters. Mol. Biol. Cell *15*, 3876–3890.

Sauer, M., Juranek, S.A., Marks, J., De Magis, A., Kazemeier, H.G., Hilbig, D., Benhalevy, D., Wang, X, Hafner, M., and Paeschke, K. (2019). DHX36 prevents the accumulation of translationally inactive mRNAs with G4-structures in untranslated regions. Nat. Commun. *10*, 2421. doi:10.1038/s41467-019-10432-5

Shapiro, E., Biezuner, T., and Linnarsson, S. (2013). Single-cell sequencing-based technologies will revolutionize whole-organism science. Nat. Rev. Genet. *14*, 618-630.

Shin, Y., and Brangwynne, C.P. (2017). Liquid phase condensation in cell physiology and disease. Science *357*, eaaf4382 doi: 10.1126/science.aaf4382.

Singh, A.K., Choudhury, S.R., De, S., Zhang, J., Kissane, S., Dwivedi, V., Ramanthan, P., Petric, M., Orsini, L., Hebenstreit, D., and Brogna, S. (2019). The RNA helicase UPF1 associates with mRNAs co-transcriptionally and is required for the release of mRNAs from gene loci. eLife *8*, e41444.

Taghbalout, A., & Rothfield, L. (2008). RNaseE and RNA helicase B play central roles in the cytoskeletal organization of the RNA degradosome. J. Biol. Chem. *283*, 13850–13855.

Tauber, D., and Parker, R. (2019). 15-Deoxy-$\Delta^{12,14}$-prostaglandin J2 promotes phosphorylation of eukaryotic initiation factor 2α and activates the integrated stress response. J. Biol. Chem. *294*, 6344-6352.

Tourrière, H., Chebli, K., Zekri, L., Courselaud, B., Blanchard, J.M., Bertrand, E., and Tazi, J. (2003). The RasGAP-associated endoribonuclease G3BP assembles stress granules. J. Cell Biol. *160*, 823–831.

Trcek, T., Grosch, M., York, A., Schroff, H., Lionnet, T., and Lehmann, R. (2015). Drosophila germ granules are structured and contain homotypic mRNA clusters. Nat. Commun. *6*, 7962.

Tu, Y.T., & Barrientos, A. (2015). The Human Mitochondrial DEAD-Box Protein DDX28 Resides in RNA Granules and Functions in Mitoribosome Assembly. Cell Rep. *10*, 854–864.

Van Treeck, B., and Parker, R. (2018). Emerging Roles for Intermolecular RNA-RNA Interactions in RNP Assemblies. Cell *174*, 791-802.

Van Treeck, B., Protter, D.S.W., Matheny, T., Khong, A., Link, C.D., and Parker, R. (2018). RNA self-assembly contributes to stress granule formation and defining the stress granule transcriptome. Proc. Natl. Acad. Sci. USA *115*, 2734-2739.

West, J.A., Mito, M., Kurosaka, S., Takumi, T., Tanegashima, C., Chujo, T., Yanaka, K., Kingston, R.E., Hirose,T., Bond, C., *et al*. (2016). Structural, super-resolution microscopy analysis of paraspeckle nuclear body organization. J. Cell Biol. *214*, 817-30.

Youn, J.Y., Dunham, W.H., Hong, S.J., Knight, J.D.R., Bashkurov, M., Chen, G.I., Bagci, H., Rathod, B., MacLeod, G., Eng, S.W.M., *et al*. (2018). High-density proximity mapping reveals the subcellular organization of mRNA-associated granules and bodies. Mol. Cell *69*, 517-532.

Methods

In vitro transcription of RNAs

Drosophila nos, *pgc*, *ccr4*, and *cycB* T7 transcription plasmids were procured from the Drosophila Genomics Research Center (DGRC; Bloomington, IN). The m*Firre*3.1 T7 transcription plasmid was generously provided by the Rinn lab at CU Boulder. The CUG repeat RNA construct was generously provided by the Disney lab (Scripps Research Institute). Plasmids were linearized via restriction digestion with BamHI-HF for the *Drosophila* RNAs, Afe1 for luciferase, and Kpn1-HF for *Firre* (enzymes from New England Biolabs (NEB)). The CUG repeat construct was linearized with HindIII-HF (NEB). Restriction digestion reactions were performed according to the manufacturers' recommendations. Following linearization, plasmid DNA was recovered with ethanol precipitation followed by resuspension in TE buffer (10 mM Tris HCl, 1 mM EDTA, pH 8.0). See Table S3 for plasmid list.

In vitro transcription of fluorescent RNAs was performed using the T7 MEGAscript kit (Ambion) according to the manufacturer's recommendations with the following modification: Addition of unlabeled UTP was reduced by 25% and an equal amount of fluorescently labeled UTP (fluorescein-12-UTP or cyanine-5-UTP, Enzo Life Sciences) was added in to the reaction mixture. Following transcription, DNA was removed by treating with TURBO DNase I (Ambion) according to the manufacturer's recommendations. RNA was recovered by sequential acid phenol/chloroform and chloroform extractions, followed by precipitation in isopropanol and NH_4OAc. RNA recovery was quantified via UV-Vis at 260 nm using a Nanodrop 2000 device (Thermo-Fischer). Proper RNA sizes were validated through either denaturing gel electrophoresis or Agilent TapeStation RNA ScreenTape analysis (performed by the BioFrontiers Next-Generation Sequencing Core Facility). Recovered RNA was resuspended in RNase-free water (Invitrogen) or TE and stored at –80°C. Working 100 µg/ml stocks were created as needed by diluting appropriately into RNase-free water and kept at –80°C.

Homopolymer condensation

Homopolymer RNAs were purchased as salts from Amersham Pharmacia Biotech, Inc. (polyA, polyC, and polyU) and Sigma-Aldrich (polyU) and made into 25 mg/mL stock solutions in TE or RNase-free water, then kept at –80°C. Working 5 mg/mL stock solutions were prepared by diluting into RNase-free water. These working stocks were stored at –80°C or –20°C. The fluorescently-labeled oligonucleotides were purchased from IDT and resuspended, from which 2 µM stock solutions were made and stored at –80°C. An initial aliquot of the fluorescently-labeled PTR (*p*olypyrimidine *t*ract *R*NA; Table S1) was purchased from IDT and was stored at –80°C as a 2 µM stock solution.

To form homopolymer condensates for the short RNA localization experiments, homopolymer RNA was condensed as described previously (Van Treeck et al., 2018), with the addition of 200 nM fluorescent RNA oligos in the condensation mix. To localize *in vitro* transcribed RNAs, homopolymer RNA was condensed with the transcribed RNA in the same manner as above, but instead mixed with 150 mM NaOAc, 600 mM NaCl, 1 mM $MgCl_2$, and 10% w/v PEG 3350 (all in RNase-free water) to a final homopolymer concentration of 0.4 mg/ml and a final mRNA/lncRNA concentration of 10 µg/ml, yielding an approximate pH of 7 as assessed by litmus paper.

Repeat RNA (reRNA) condensation

CUG repeat foci were prepared by condensing 200 µg/ml of fluorescein-labeled *DMPK*$^{\text{Exons 11-15}}$-CUG_{590} RNA as in Jain and Vale (2017) in the presence or absence of 10 µg/ml Cy5-labeled *in vitro* transcribed RNAs or 200 nM PTR-Cy3. Briefly, RNAs were mixed together in a buffer of 10 mM $MgCl_2$, 10 mM Tris HCl pH 6.8, and 25 mM NaCl, and subsequently denatured for 3 min at 95°C then cooled at ~4°C/min to 37°C in a thermocycler. Afterwards, condensates were immediately imaged.

Stress granule isolation and RNA recruitment

To test the ability of SGs to recruit *in vitro* transcribed RNAs, SGs were purified as follows: First, GFP-G3BP1 U-2 OS cells were seeded at ~40% confluency and then grown to ~80% confluency, after which the media was replaced and the cells were stressed with 500 µM arsenite for 60 min. Afterwards, the cells were washed, pelleted, and flash-frozen in liquid N_2, then stored at –80°C for up to a week. SGs were isolated as in Khong et al. (2017) to produce SG-enriched fraction. No affinity purification was performed. Other cellular debris was removed from the SG-enriched supernatant through both vigorous pipetting and by passing the supernatant through a 25G 5/8 needle, accompanied by quick spins. RNA recruitment to SGs was assessed by incubating 10 µg/mL Cy5-labeled luciferase RNA with SGs for 10 minutes at room temperature, followed by imaging.

RNA condensate dilution assays

To test the stability of RNA assemblies under dilution, *pgc*-decorated polyA droplets were prepared as above and incubated 2 hours. Thereafter, they were subjected to spinning disk confocal time-lapse microscopy. Every 18 sec, an image was taken in each channel in a 4x4 grid of adjacent frames using the Nikon Elements software "Large Image" tool. These images were automatically stitched together. Dilutions were performed while imaging was ongoing. In between imaging timepoints, TE buffer was quickly added dropwise (so as to only minimally disturb assemblies) to a tenfold final dilution. The very next imaging timepoint was taken to be $t = 0$ for quantitative analysis.

RNA crosslinking assays

To observe RNA-condensate-associated RNA-RNA interactions, 4'-aminomethyltrioxsalen (AMT) crosslinking was performed (Frederikson and Hearst, 1979). AMT was procured from Santa Cruz Biotechnology and solubilized to a final concentration of 1 mg/ml in DMSO. AMT stocks were stored at –20°C. Since AMT crosslinks pyrimidine residues, condensation-crosslinking experiments were performed using polyA condensates.

In condensation-crosslinking experiments, RNA was demixed in the appropriate condition, but with the addition of 100 µg/ml AMT. Following incubation, RNA was crosslinked by irradiating 15 min with 366 nm UV light. Afterwards, samples were diluted 1:1.7 in TE and RNA was recovered by precipitation in 2 M LiCl. If RNA sample concentrations were low (e.g., tanglet conditions), 0.4 mg/ml polyA homopolymer RNA was added post- crosslinking and pre-precipitation as a carrier in order to promote efficient recovery.

Denaturing gel electrophoresis

Denaturing gel electrophoresis was performed to analyze fluorescent and crosslinked RNAs. RNA samples were mixed with either 6x formaldehyde loading dye (Ambion) or 2x formamide loading dye (95% deionized formamide, 0.025% w/v bromophenol blue, 5 mM EDTA) and denatured by incubation at 70°C for 15 min, followed by incubation on ice for 3 min. Samples were run in freshly-prepared 1% agarose, 1% formaldehyde denaturing gels in fresh 1x MOPS buffer (20 mM MOPS, 5 mM NaOAc, 1 mM EDTA, pH 7) at 4-10 V/cm for 2.5-4 hours.

Denaturing gels were imaged using a Typhoon FLA 9500 imaging system (GE) set to visualize the appropriate fluorescence signal from fluorescently-labeled RNAs. Crosslinking efficacies were quantified in ImageJ by measuring the integrated intensities of the monomer bands and higher-weight bands, subtracting the average of 10-15 background measurements, and dividing the sum of the corrected higher-weight integrated intensities by the sum of all band integrated intensities. In symbols:

$$\mathrm{CE} = \frac{\sum_{n=2}^{N} I_n}{\sum_{n=1}^{N} I_n} \times 100\%\,,$$

where I_n is the (background-corrected) integrated intensity of the band corresponding to the RNA n-mer, N is the highest order band observed in a given sample, and CE is the crosslinking efficacy.

Total RNA isolation and *in vitro* decondensase assays

Saccharomyces cerevisiae was grown to and OD600 of 0.8 AU and was lysed with 425-600 µm glass beads (Sigma-Aldrich) and vortexing for 10 minutes in a 50 mL conical tube. RNA was extracted by using TRIzol reagent (Ambion) according to manufacturer's instructions. Purified RNA concentration was determined via UV-Vis at 260 nm using a Nanodrop 2000 device (Thermo).

To assess the ability of eIF4A1 to decondense RNA *in vitro*, 10 µM recombinant eIF4A1 was mixed together in with 150 µg/mL yeast total RNA extracts, 200 µM fluorescent PTR (IDT), and either 1 mM ATP or ADPNP (Sigma-Aldrich) in 150 mM KOAc, 1 mM $MgCl_2$, 0.223 mM spermine tetrahydrochloride, 1.34 mM spermidine trihydrochloride, and 8% w/v PEG 3350 (pH ~7, 37°C) in a glass bottom-96 well plate. Polyamine levels recapitulate physiological concentrations. For each reaction, RNA condensate formation was observed after initial RNA addition by DIC and TRITC channels over 60 minutes with images taken every 5 minutes. %Droplet area was analyzed using "Particle finder" in ImageJ.

Cell culture, drug treatments, and transfections

All cell lines were grown and maintained at 37°C and 5% CO_2. Cells were grown in Dulbecco's modified Eagle's medium (DMEM) with 10% fetal bovine serum (FBS) and 1% penicillin/streptomycin mix.

For drug treatments or transfections, cells were seeded at 10^5 cells/mL and were allowed to adhere overnight. For siRNA experiments, cells were transfected with 50 nM of scrambled or

eIF4A1 siRNA (see Table S1) using Interferin (polyPLUS) according to the manufacturer's instructions for 48 h before SG induction. For overexpression experiments, cells were transfected with control (pcDNA3.1, Addgene) or pcDNA3.1-Myc-eIF4A1 (Addgene) plasmids (see Table S3) for 48 h prior to SG induction or pmCherry (control) or pmCherry-DDX19A plasmids for DDX19A OE.

To induce SGs, arsenite (500 µM in H_2O, Sigma-Aldrich), hippuristanol (Hipp., 300 nM or 1 µM in DMSO), or Pateamine A (PatA, 100 nM in DMSO) were added and cells were incubated at 37°C for the allotted times indicated in each assay. To deplete ATP, cells were incubated with 2-deoxy-D-glucose (2DG, 200 mM in H_2O, Sigma-Aldrich) and carbonyl cyanide *m*-chlorophenyl hydrazine (CCCP, 100 µM in DMSO, Sigma-Aldrich). For ribopuromycinylation assays, cells were incubated at 37°C with puromycin (10 µg/mL in H_2O, Sigma-Aldrich) 5 minutes prior to fixation or lysis.

Immunoblotting

Following drug treatment or transfection, cells were washed with 37°C phosphate buffered saline (PBS) and lysed with NP-40 lysis buffer (50 mM Tris-HCl pH 8.0, 150 mM NaCl, 1% NP-40 and protease inhibitor cocktail (Thermo Scientific)). Cell lysates were rocked at 4°C for 30 minutes, and then clarified by centrifugation (13K RPM for 60 s). 4x Nu-PAGE sample buffer was added to lysates to a final concentration of 1x, samples were boiled for 5 minutes at 95°C, and then loaded into 4-12% Bis-Tris Nu-PAGE gel and transferred to a nitrocellulose membrane. Membranes were blocked with 5% BSA in Tris-buffered saline with 0.1% Tween-20 (TBST) for an hour and then incubated with primary antibody overnight at 4°C. Membranes were washed 3x with TBST, then incubated at room temperature for 2 hours in 5% BSA in TBST. Membranes were washed 3x again in TBST and antibody detection was achieved by rocking membranes in Pierce ECL western blotting substrate for 5 minutes.

Chemiluminescence was visualized on an Image Quant LAS 4000 (GE). Protein band densities were quantified in ImageJ.

Immunofluorescence (IF) and fluorescence *in situ* hybridization (FISH)

Cells were prepared as described as stated above except grown on No. 1.5 glass coverslips (Thermo). Sequential IF/FISH or IF/smFISH was performed as previously described (*5*, *27*). When IF was performed in the absence of FISH, fixed U-2 OS cells were instead blocked with 5% BSA in PBS for 1 hour prior to IF and the antibodies were diluted in 5% BSA in PBS.

Alternatively, fixed cells were simultaneously blocked and permeabilized with 5% BSA in PBS-T (0.1% Triton-X-100) for 1 hour at room temperature. Thereafter, coverslips were incubated with primary antibody (1:500) overnight at 4°C in 1% BSA in PBS-T. Coverslips were then washed 3X with PBS and incubated with secondary antibody (1:1000) at room temperature for 2 hours in 1% BSA in PBS-T.

The primary antibodies used for immunofluorescence (IF) include mouse anti-G3BP (5 µg/mL, ab56574(Abcam)), rabbit anti-DDX1 (1:100, 11357-1-AP (Proteintech)), and rabbit anti-

eIF4A1 (100 µg/mL, ab31217(Abcam)) and the appropriate secondary antibodies used were goat anti-mouse FITC antibody (1:1000, Abcam (ab6785)), and donkey anti-rabbit Alexa Fluor 555 conjugate antibody (1:500, Abcam (ab150062).

NORAD-Quasar670 smFISH probes were custom made using Stellaris® RNA FISH probe Designer (Biosearch Technologies, Inc., Petaluma, CA). The probe sequences are listed in Table S2. *AHNAK*-Quasar670, *TFRC*-Quasar570, and *POLR2A*-Quasar570 probes were purchased premade directly from Biosearch Technologies and resuspended according to the manufacturer's recommendations. AHNAK smFISH probe sequences are in Khong et al., 2017. Oligo(dT)-Cy3 probes were purchased from IDT.

Microscopy

Fixed U-2 OS cells stained by IF and/or smFISH, purified SGs, CUG repeat RNA foci, and homopolymer condensates were imaged using a widefield DeltaVision Elite microscope with a 100x NA 1.5 oil objective using a PCO Edge sCMOS camera and SoftWoRx software (GE).

Condensate dilution and helicase assays were imaged using an inverted Nikon Ti Eclipse spinning disk confocal microscope equipped with an environmental chamber and Nikon Elements software. Helicase assay imaging was performed at 37°C. All spinning disk confocal images were acquired with a 100x NA 1.5 oil objective and a 2x Andor Ultra 888 EMCCD camera.

Fluorescence recovery after photobleaching (FRAP)

FRAP assays were performed using an inverted Nikon A1R laser scanning confocal microscope equipped with an environmental chamber, a 100x NA 1.5 oil objective, and Nikon Elements software. At least three images were prior to photobleaching followed imaging over the course of recovery. PolyA/*pgc* FRAP was performed at room temperature.

To analyze recovery, the mean intensity of each bleached region was quantified in ImageJ, and recovery intensities were normalized to the mean of three pre-bleach measurements. Mobile fractions φ_M were computed by subtracting the minimum normalized mean intensity I_0 from the normalized endpoint intensity I_F: $\varphi_M = I_F - I_0$.

Image analysis

Single molecule FISH analysis was performed using Imaris (Bitplane) as in Khong et al. (2017).

G3BP1, eIF4A1, and oligo(dT) partitioning were quantified using Imaris Imaging Analysis software (Bitplane). In order to measure partitioning, first, the nuclei were masked using the DAPI source channel. Second, individual cells were segmented by creating a region of interest (manually determined) around a single cell using the surface creation wizard. Mean cellular fluorescence intensities for G3BP1, eIF4A1, and oligo(dT) were then obtained under the results tab. Third, SGs were identified using the G3BP1 fluorescent source channel with Imaris Cell Creation wizard with the following parameters (0.0406 µm filter width, manually-

determined thresholding, and ≥ 1 voxel). Once SGs were identified by the cell creation wizard, they are then converted to surfaces in order to extract mean fluorescence intensities for G3BP1, eIF4A1 and oligo(dT) inside stress granules. Partitioning was then calculated by taking the ratio of the mean fluorescence intensity in SG to the mean fluorescence intensity in the cell. 20 cells were counted for each sample. For more detailed information, please see Khong et al. (2017).

Line analysis was performed using ImageJ (FIJI). A straight line was drawn across a stress granule using G3BP1 as a source channel. The line is then saved as an ROI. The ROI was then pasted on the corresponding eIF4A1 or DDX1 source channel. Line intensities were then extracted in both channels using the "Plot Profile" tool. Stress granule boundaries (in each source channel) were determined by an intensity threshold halfway between the maximum and minimum intensity values for each source channel. Fifty linescan analyses were performed for each experiment.

Measurements of SG area or PB area per cell area were quantified using the "Particle Finder" tool in ImageJ. The percent of cells with SGs was quantified using the "Count" tool in ImageJ. The fluorescence intensity of puromycin-labeled nascent peptides in individual cells was quantified as mean gray values extracted from ImageJ.

The index of dispersion (DI) is a statistical measure of inhomogeneity in a population and is defined to be

$$\mathrm{DI} = \frac{\sigma^2}{\mu},$$

where σ^2 is the variance of the population distribution (with σ being the population standard deviation) and μ is the mean value. For example, particles in an ideal solution exhibit a dispersion index of 1, as they are Poisson distributed, and substantially higher values indicate particle-particle interactions in that context. Here, dispersion indices were used to quantify inhomogeneity in fluorescence signal and infer the relative extent to which an RNA is assembled, similarly to Jain and Vale (2017).

Indices of dispersion were computed by measuring the mean fluorescence intensity and standard deviation for maximum projections of 1 μm Z-stacks or single slices in the case of the dilution experiment. An index was computed for each image using ImageJ, and the displayed index was taken to be the average of the indices for all the separate images. The standard deviations for the distribution of index values for a given set of conditions were used to calculate 95% confidence intervals.

Statistical analysis

Statistical significance was assessed using the Student's *t*-test with two tails.

Estimates of eIF4A1 levels per mRNA.

For HeLa and U-2 OS cells we used published values for eIF4A1 from quantitative mass spectroscopy, 1.7×10^7 and 2.2×10^6, respectively (Itzhak et al., 2016; Beck et al., 2011), and mRNA levels for U-2 OS cells, ~330,000 (Khong et al., 2017). Although previous estimates suggest HeLa cells might contain 200,000 mRNAs per cell (Shapiro et al., 2013) we utilized an estimate of 330,000 mRNAs per cell to be conservative in our estimations. These calculations indicate a ratio of 6.7 eIF4A1 molecules/mRNA to 51 eIF4A molecules/mRNA in U-2 OS and HeLa cells respectively.

Figure 1

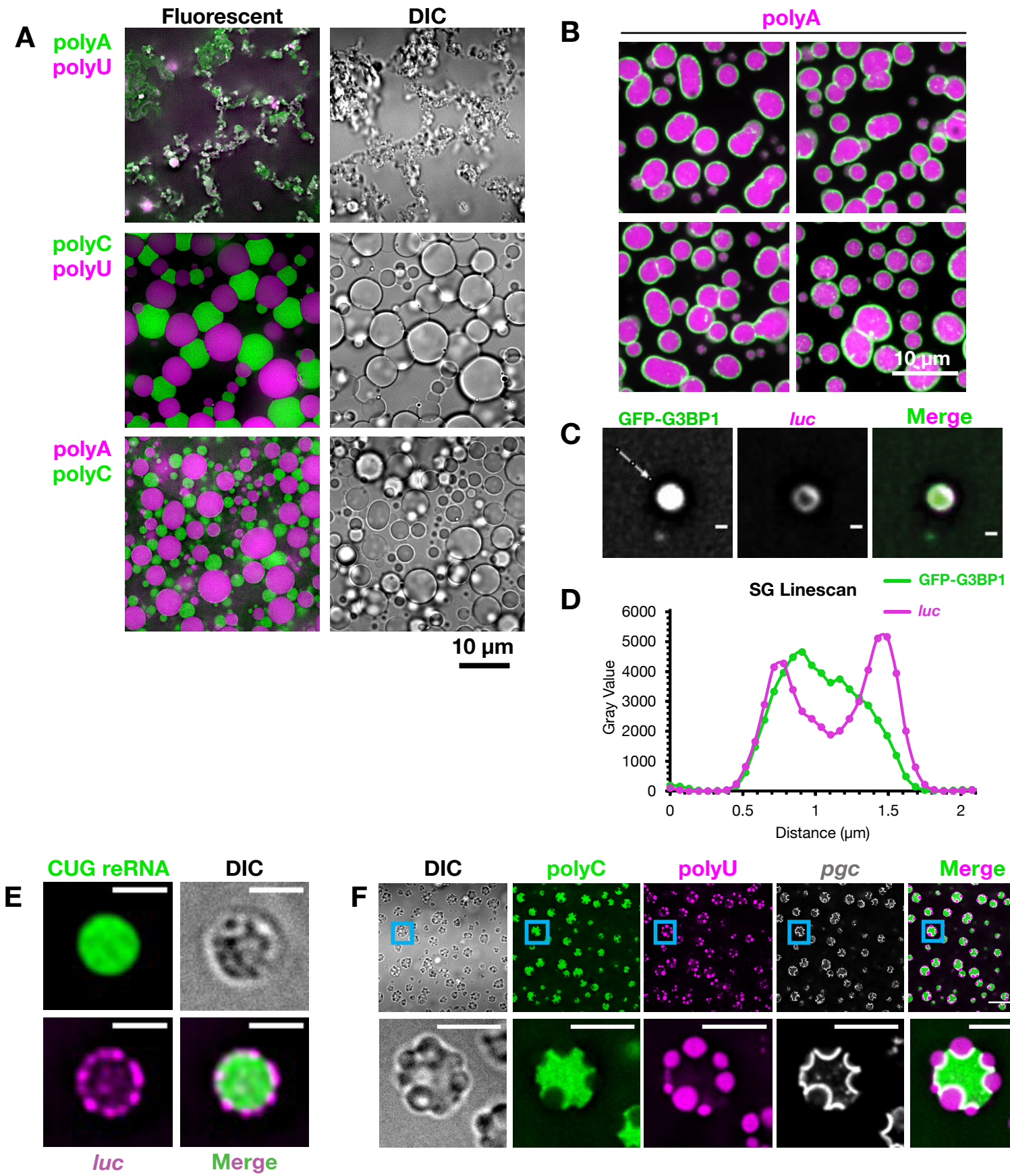
A
Fluorescent
DIC
polyA
polyU
polyC
polyU
polyA
polyC
10 µm
B
polyA
10 µm
C
GFP-G3BP1
luc
Merge
D
SG Linescan
GFP-G3BP1
luc
Gray Value
6000
5000
4000
3000
2000
1000
0
0
0.5
1
1.5
2
Distance (µm)
E
CUG reRNA
DIC
luc
Merge
F
DIC
polyC
polyU
pgc
Merge

Figure 1. Surface free energy drives the assembly and organization of RNA. (A) Pairwise combinations of homopolymers were condensed together and visualized with fluorescent antisense oligos (*see also Figure S1A-S1C*, *Movie S1*). (B) PolyA assemblies (labeled by U_{19}-Cy3) were condensed with fluorescent *in vitro* transcribed RNAs (*see also Figure S1D*). (C) Purified SG cores containing GFP-G3BP1 were incubated with fluorescent *luc* RNA. Scale bars are 500 nm. (D) Line profile of (C) along the line denoted by the white arrow. (E) A fluorescent myotonic dystrophy repeat RNA (reRNA) containing exons 5-11 of *DMPK* and ~590 CUG repeats was condensed with fluorescent *luc*. Scale bars are 2 µm. (F) Fluorescent *pgc* was condensed with polyC and polyU (and the corresponding fluorescent antisense oligos), localizing to the polyC/polyU interface. Scale bars are 5 µm

Figure 2

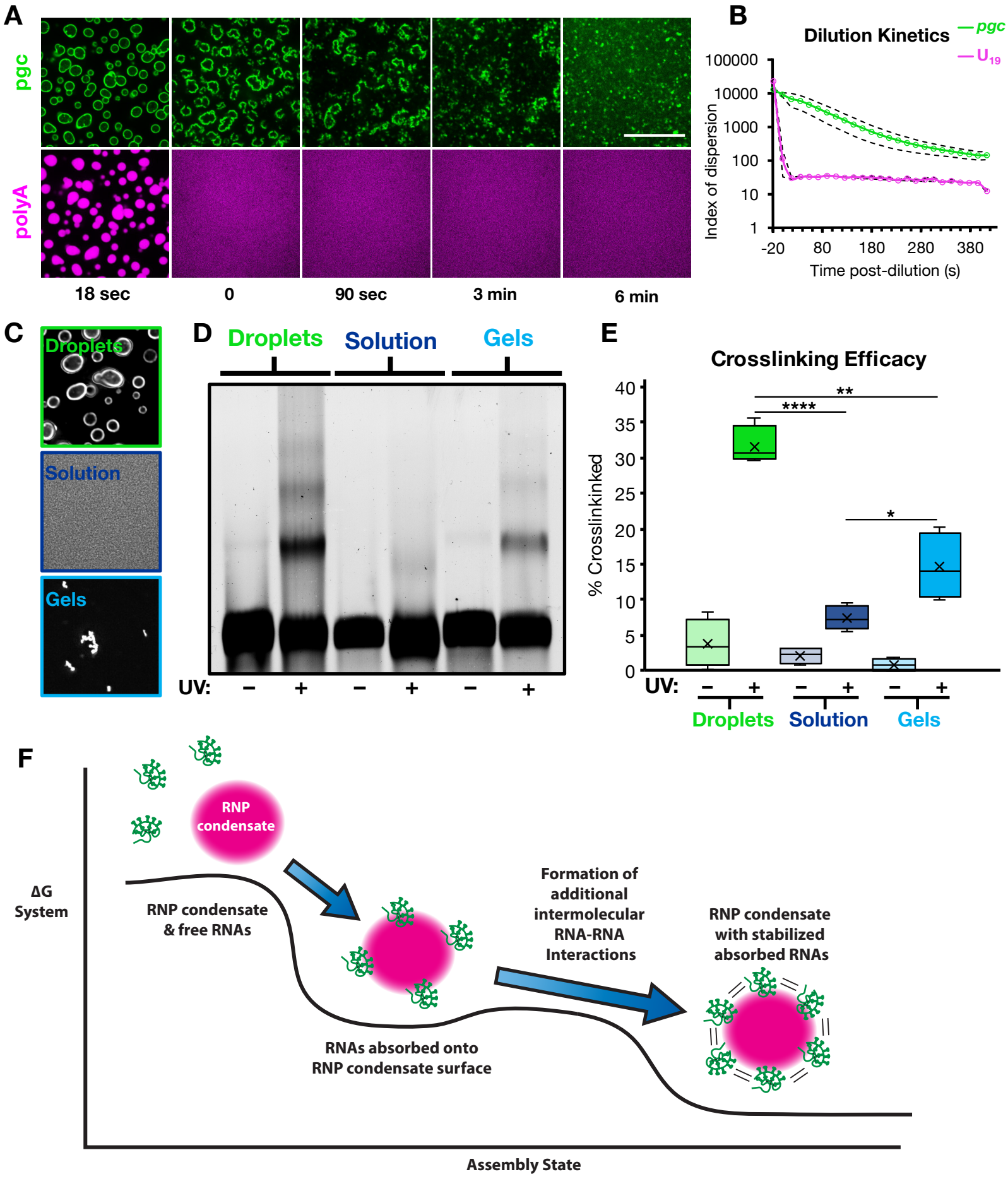
A
pgc
polyA
18 sec
0
90 sec
3 min
6 min
B
Dilution Kinetics
pgc
U19
Index of dispersion
100000
10000
1000
100
10
1
-20
80
180
280
380
Time post-dilution (s)
C
Droplets
Solution
Gels
D
Droplets
Solution
Gels
UV:
−
+
−
+
−
+
E
Crosslinking Efficacy
% Crosslinkinked
40
35
30
25
20
15
10
5
0
**
****
*
UV:
−
+
−
+
−
+
Droplets
Solution
Gels
F
RNP condensate
ΔG System
RNP condensate & free RNAs
RNAs absorbed onto RNP condensate surface
Formation of additional intermolecular RNA-RNA Interactions
RNP condensate with stabilized absorbed RNAs
Assembly State

Figure 2. RNA condensate surface localization stabilizes intermolecular RNA-RNA interactions. (A) Fluorescent *pgc* was condensed with polyA and fluorescent U_{19}, and the condensates were subjected to 1:10 dilution in TE buffer. Scale bar is 20 µm (*see also Figure S2*). (B) Quantification of (A) as an index of dispersion, showing the persistence of *pgc* shell assemblies over time. Dashed lines are 95% confidence intervals. *See also Movie S2*. (C) Images of the crosslinking conditions showing *pgc* on droplets, in solution, and as gels. (D) Representative fluorescence denaturing gel. (E) Quantification of (D), showing that RNA condensate surfaces enhance intermolecular RNA interactions in comparison to solvated RNA or RNA condensed alone. X represents the mean. $*p<0.05$, $**p<0.01$, $****p<10^{-4}$. (F) Model energy diagram for intermolecular RNA-RNA interactions on RNP condensate surfaces. Surface localization increases the local [RNA], promoting intermolecular RNA-RNA interactions and further stabilizing the system.

Figure 3

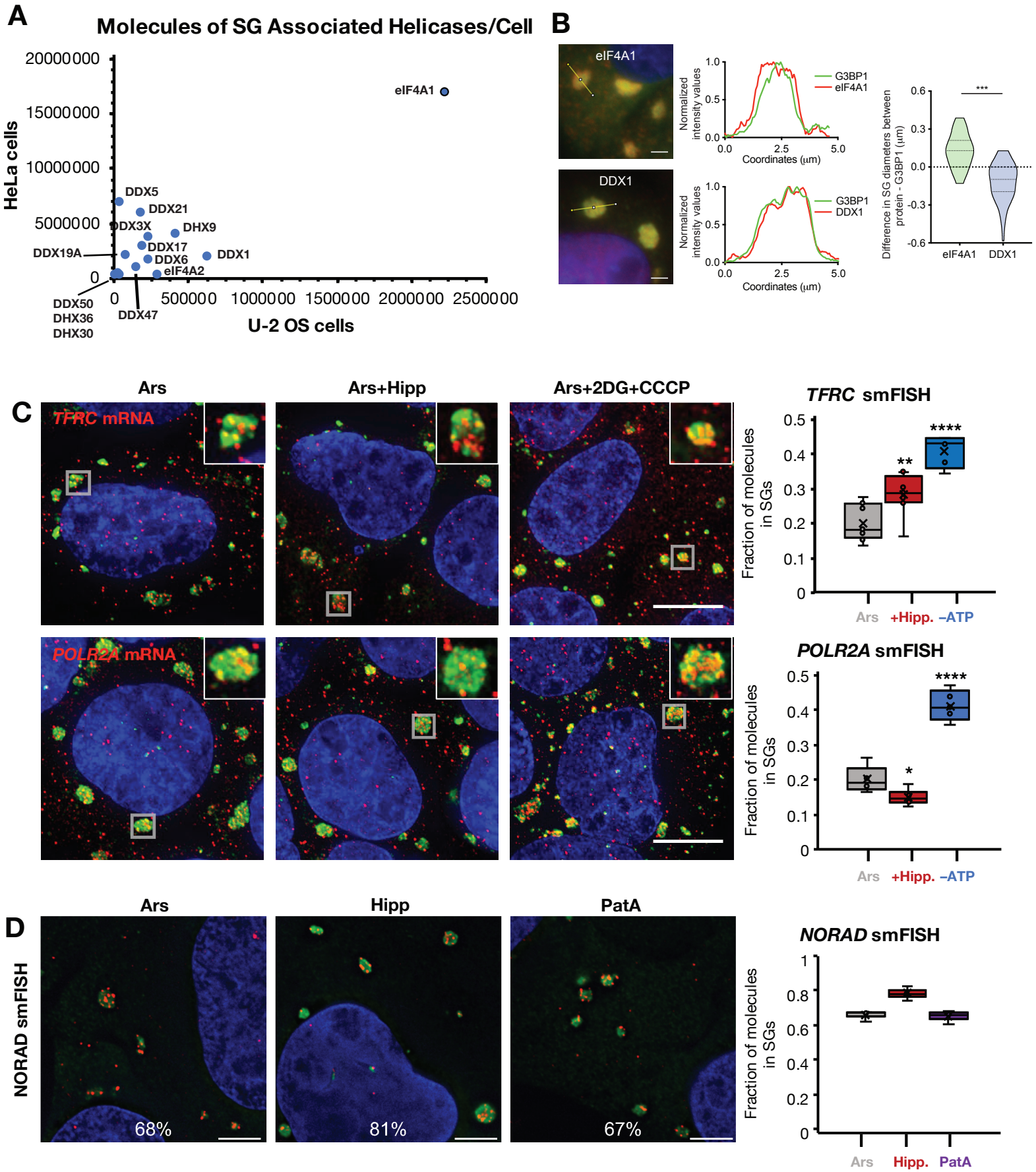
A
Molecules of SG Associated Helicases/Cell
HeLa cells
U-2 OS cells
eIF4A1
DDX5
DDX21
DDX3X
DHX9
DDX17
DDX19A
DDX6
DDX1
eIF4A2
DDX50
DHX36
DHX30
DDX47
B
eIF4A1
DDX1
Normalized intensity values
Coordinates (μm)
G3BP1
eIF4A1
DDX1
Difference in SG diameters between protein - G3BP1 (μm)
***
C
Ars
Ars+Hipp
Ars+2DG+CCCP
TFRC mRNA
POLR2A mRNA
TFRC smFISH
POLR2A smFISH
Fraction of molecules in SGs
Ars
+Hipp.
–ATP
D
NORAD smFISH
Ars
Hipp
PatA
68%
81%
67%
NORAD smFISH
Fraction of molecules in SGs
Ars
Hipp.
PatA

Figure 3. eIF4A helicase activity limits RNA recruitment to SGs. (A) Scatterplot of SG-associated helicase abundance in U-2 OS vs. HeLa cells. (B) Immunolocalization of eIF4A1 in SGs. eIF4A1 extends past the SG periphery as compared to DDX1, which co-extends with G3BP1. Scale bars are 2 µm. (C) smFISH images and quantification of SG enrichment for *TFRC* and *POLR2A* mRNAs in U-2 OS cells treated with 60' arsenite, then 30' DMSO, hippuristanol, or 2DG and CCCP. Gray boxes denote the SGs in the insets. SGs are visualized by anti-PABPC1 IF. Scale bars are 20 µm. (D) *NORAD* lncRNA smFISH images and quantification in U-2 OS cells treated with arsenite, hippuristanol, or PatA. SGs are visualized by anti-G3BP1 IF. *$p<0.05$, **$p<0.01$, ***$p<10^{-3}$, ****$p<10^{-4}$. *See also Figure S3*.

Figure 4

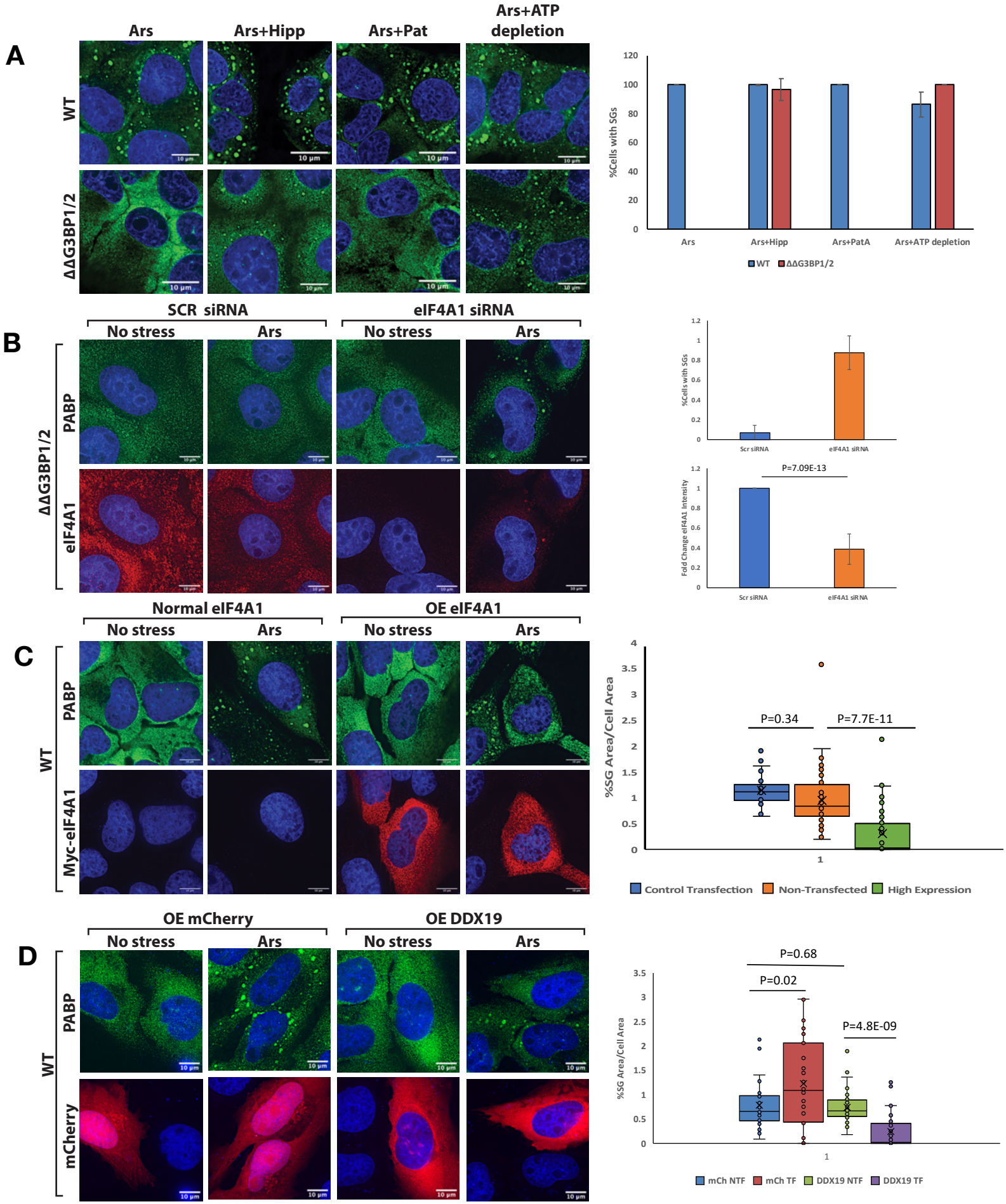
A
Ars
Ars+Hipp
Ars+Pat
Ars+ATP depletion
WT
ΔΔG3BP1/2
10 µm
%Cells with SGs
120
100
80
60
40
20
0
Ars
Ars+Hipp
Ars+PatA
Ars+ATP depletion
WT
ΔΔG3BP1/2
B
SCR siRNA
eIF4A1 siRNA
No stress
Ars
No stress
Ars
ΔΔG3BP1/2
PABP
eIF4A1
%Cells with SGs
Scr siRNA
eIF4A1 siRNA
P=7.09E-13
Fold Change eIF4A1 Intensity
C
Normal eIF4A1
OE eIF4A1
No stress
Ars
No stress
Ars
WT
PABP
Myc-eIF4A1
%SG Area/Cell Area
P=0.34
P=7.7E-11
Control Transfection
Non-Transfected
High Expression
D
OE mCherry
OE DDX19
No stress
Ars
No stress
Ars
WT
PABP
mCherry
%SG Area/Cell Area
P=0.68
P=0.02
P=4.8E-09
mCh NTF
mCh TF
DDX19 NTF
DDX19 TF

Figure 4. eIF4A helicase activity limits SG formation. (A) Images displaying SG formation (as assessed by PABPC1 IF) in both wildtype and ΔΔG3BP1/2 U-2 OS cells. Arsenite, alone or in combination with hippuristanol or PatA robustly induces SG formation in wild-type cells. Hippuristanol, following arsenite, can induce SG formation in ΔΔG3BP1/2, indicating that inhibition of eIF4A's helicase activity can partially restore SG formation independently of translation (*see also Figure S4A*). Additionally, arsenite followed by ATP depletion restores SGs in ΔΔG3BP1/2 cells to a greater extent than arsenite and hippuristanol, suggesting other ATP driven machines limit RNA condensation (B) siRNA knockdown of eIF4A1 (quantified by fold change in eIF4A1 intensity) in ΔΔG3BP1/2 cells restores SGs upon addition of arsenite, indicating that eIF4A1 limits SG formation. (C) Overexpression of eIF4A1 in wildtype U-2 OS cells prevents SG formation, as quantified by %SG area/Cell area in cells expressing Myc-tagged eIF4A1, compared to un-transfected neighbor cells or control transfections (*see also Figure S4B-D*). (D) Overexpression of mCherry-DDX19A can limit arsenite induced SG formation (quantified to the right by %SG area/Cell area), and these effects were not observed with mCherry expression alone, consistent with other helicases containing the eIF4A helicase core sequence functioning as decondensases (*see also Figure S4E*).

Figure 5

A

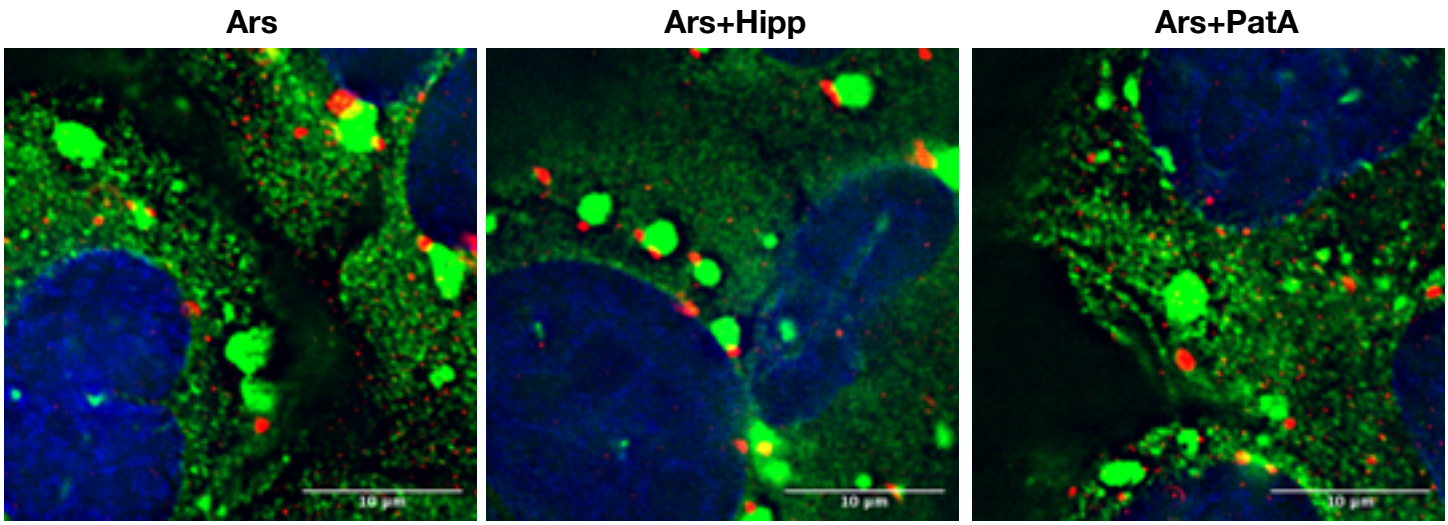

green = G3BP1
red = EDC3

B

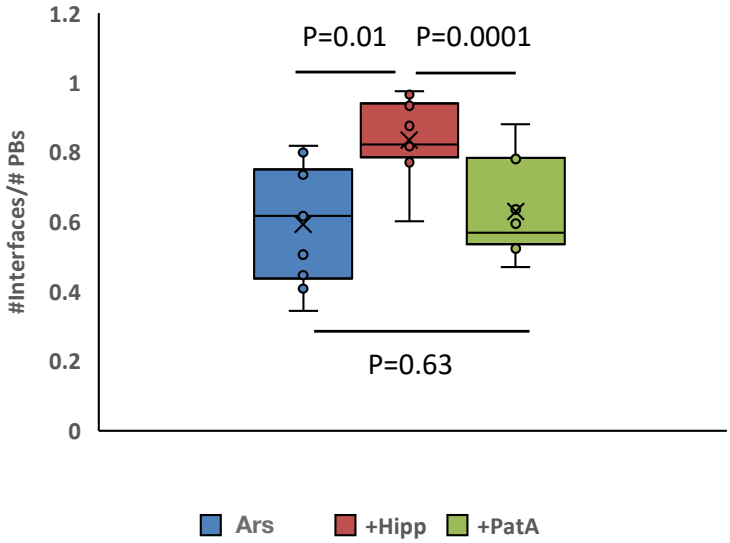

C

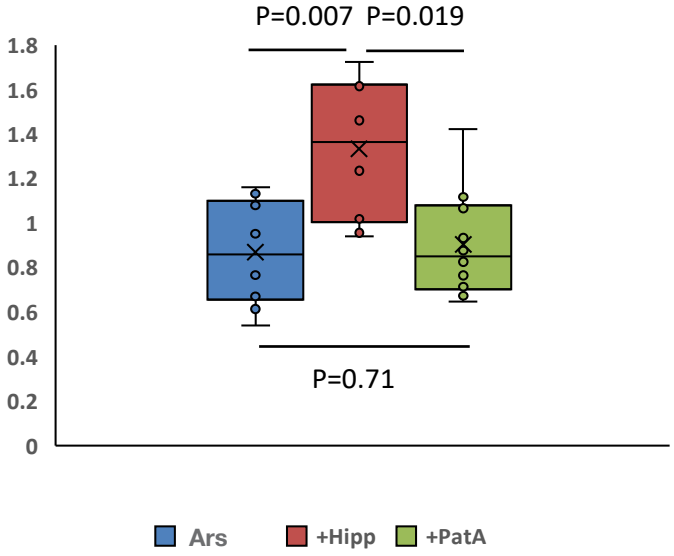

Figure 5. eIF4A helicase activity limits the docking of P bodies with stress granules. (A) The amount of PB/SG interfaces increase in the presence of arsenite in combination with hippuristanol compared to combinations of arsenite with PatA or arsenite alone. This effect holds true when normalized to the total amount of PBs (B) or SGs (C). PBs are visualized by anti-EDC3 IF and SGs by anti-G3BP1 IF.

Figure 6

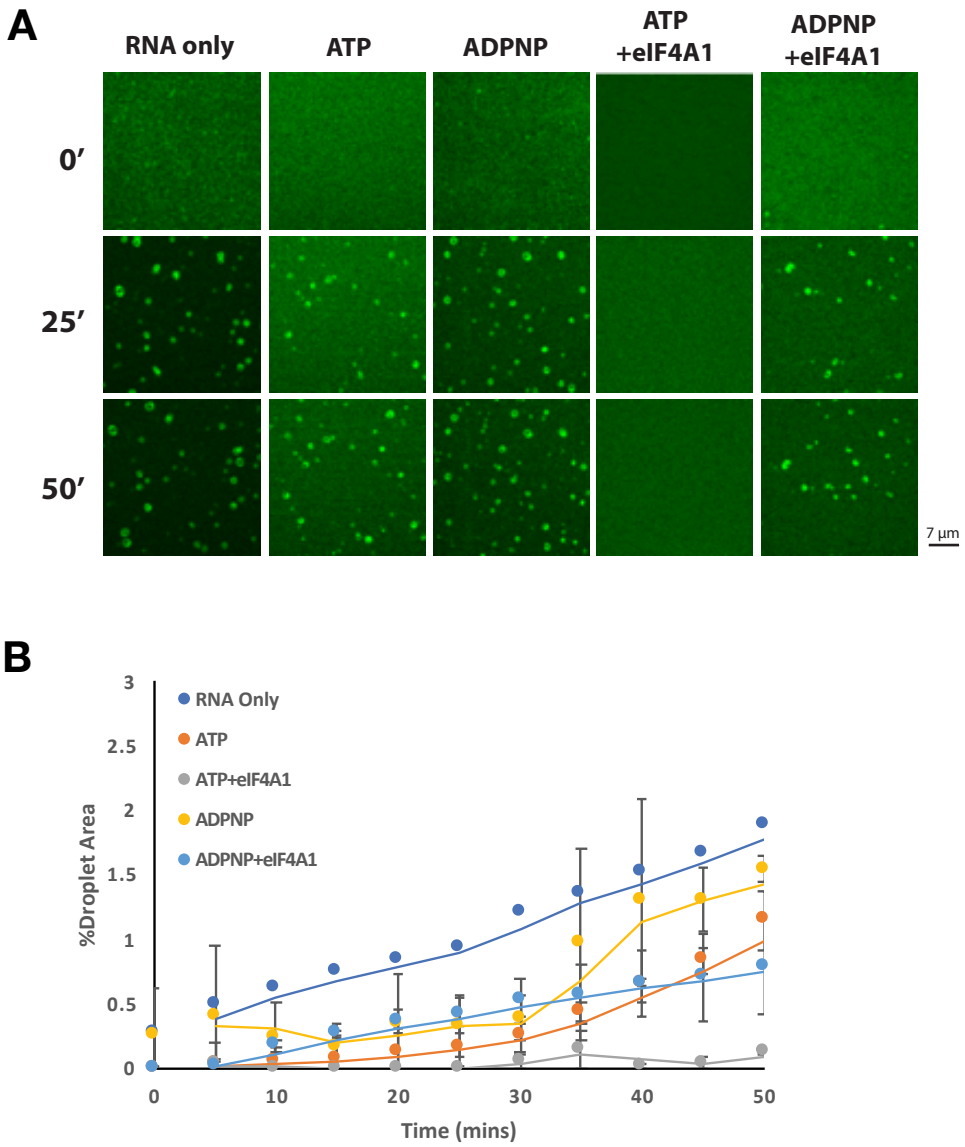
A
RNA only
ATP
ADPNP
ATP +eIF4A1
ADPNP +eIF4A1
0'
25'
50'
7 µm
B
RNA Only
ATP
ATP+eIF4A1
ADPNP
ADPNP+eIF4A1
%Droplet Area
Time (mins)
0
0.5
1
1.5
2
2.5
3
0
10
20
30
40
50

Figure 6. Recombinant eIF4A is sufficient to limit RNA condensation *in vitro*. (A) Formation of *in vitro* total RNA droplets is inhibited by eIF4A+ADPNP, and more drastically by eIF4A+ATP, suggesting that binding of eIF4A to RNA can prevent RNA condensation, with eIF4A catalytic activity being the most effective at inhibiting spontaneous RNA assembly. (B) quantification of RNA condensation kinetics as assessed by %Droplet area per time. *For DIC images see also Figure S6.*

Figure 7

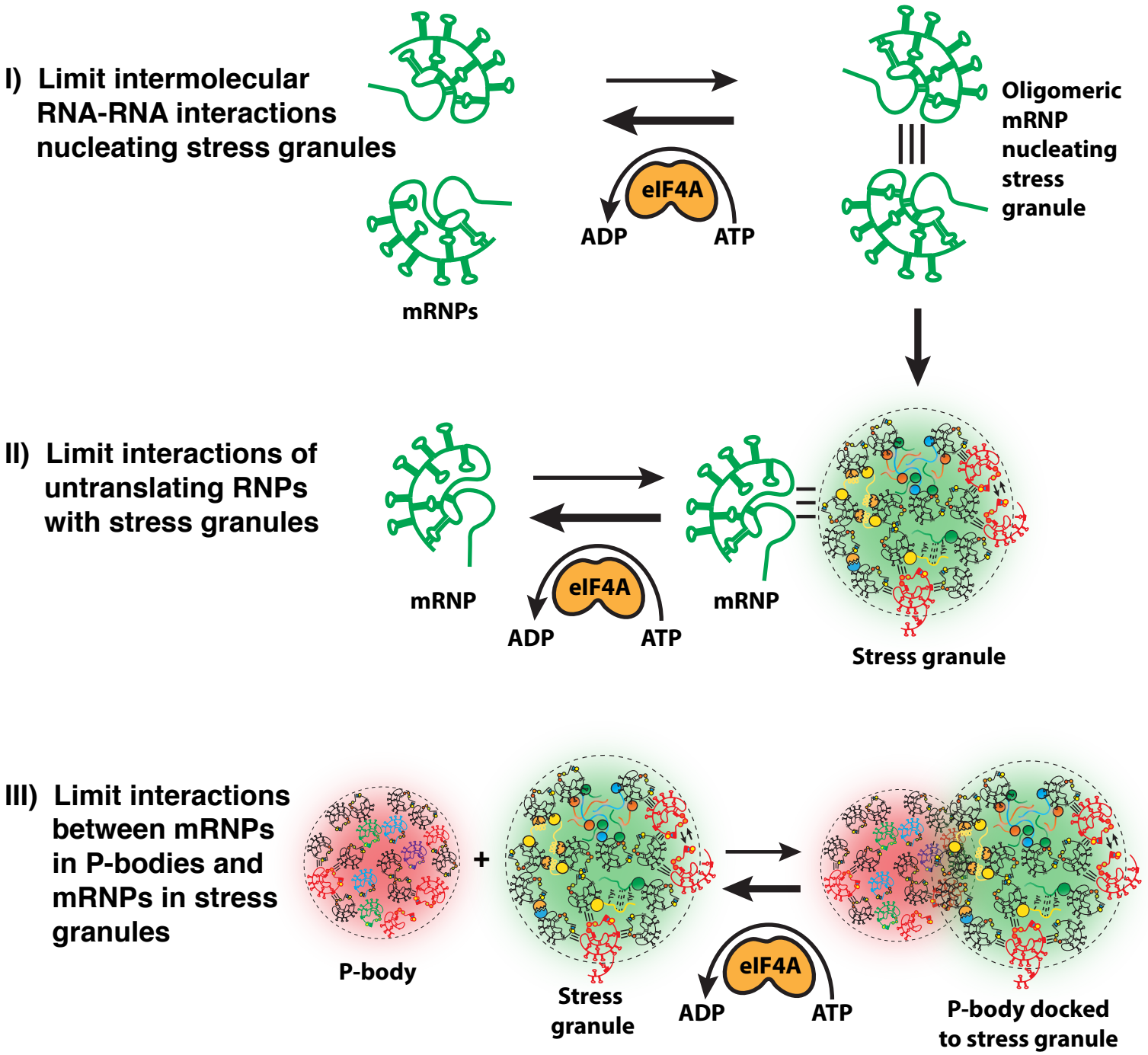
I) Limit intermolecular RNA-RNA interactions nucleating stress granules
mRNPs
eIF4A
ADP
ATP
Oligomeric mRNP nucleating stress granule
II) Limit interactions of untranslating RNPs with stress granules
mRNP
eIF4A
ADP
ATP
mRNP
Stress granule
III) Limit interactions between mRNPs in P-bodies and mRNPs in stress granules
P-body
+
Stress granule
eIF4A
ADP
ATP
P-body docked to stress granule

Figure 7. Three mechanisms by which eIF4A modulates RNA condensation.